SIN-CHN
SCIENTIFIC PRESS PTE.LTD.

Molecular & Cellular Biomechanics 2025, 22(5), 1723.
https://doi.org/10.62617/mcb1723

Article

Disinfection by-products pollution patterns and their cellular biomechanical effects

Rui Zhu*, Ya-ting Zhao, Jian-jiang Lu

School of Chemistry and Chemical Engineering, Shihezi University, Shihezi 832003, China
*** Corresponding author:** Rui Zhu, zhuruizzz0828@163.com

CITATION

Zhu R, Zhao Y, Lu J. Disinfection by-products pollution patterns and their cellular biomechanical effects. Molecular & Cellular Biomechanics. 2025; 22(5): 1723. https://doi.org/10.62617/mcb1723

ARTICLE INFO

Received: 28 February 2025
Accepted: 30 May 2025
Available online: 19 June 2025

Abstract: This study integrates water quality monitoring data analysis with cellular biomechanics research to explore the relationship between disinfection by-products (DBPs) pollution patterns and their effects on cellular mechanical properties. Using data from 12 water treatment plants across three metropolitan areas in Eastern China, we identified four distinct DBPs pollution patterns: Chlorinated THMs dominated, HAAs dominated, Brominated DBPs enriched, and Emerging DBPs enriched. Multi-parametric biomechanical analysis utilizing atomic force microscopy, microfluidic deformation tests, and cytoskeletal structure evaluation revealed that all four patterns induced concentration-dependent alterations in cellular elasticity, deformability, and migration capacity. Pattern 4 (Emerging DBPs enriched) and Pattern 3 (Brominated DBPs enriched) exhibited the strongest effects, inducing significant biomechanical changes even at environmentally relevant concentrations. HK-2 kidney cells demonstrated the highest sensitivity among tested cell lines, consistent with epidemiological evidence linking long-term DBPs exposure to increased kidney cancer risk—an important public health concern. Canonical correlation analysis established systematic relationships between DBPs characteristics and specific biomechanical responses. These findings highlight potential mechanisms underlying DBPs-associated health risks and suggest that cellular biomechanical parameters could serve as sensitive early indicators of DBPs toxicity, potentially addressing a critical gap in current risk assessment approaches that rely primarily on high-dose cytotoxicity endpoints. The established pattern-specific relationships provide important insights for targeted water treatment strategies and monitoring approaches focusing on emerging unregulated DBPs.

Keywords: disinfection by-products; pattern recognition; cellular biomechanics; water quality monitoring; toxicity assessment

1. Introduction

1.1. Formation of drinking water disinfection by-products and health risks

Water disinfection is one of the most successful public health interventions worldwide; however, disinfectants react with natural organic matter and halogen ions to form disinfection by-products (DBPs) [1]. Since the 1970s, more than 700 DBPs have been identified, including trihalomethanes (THMs), haloacetic acids (HAAs), haloacetonitriles (HANs), haloketones (HKs), and halobenzoquinones (HBQs) [2,3]. Recent studies indicate that emerging unregulated DBPs may possess higher cytotoxicity and genotoxicity than regulated ones [3,4]. The formation of DBPs is influenced by raw water quality, disinfection parameters, and environmental conditions, leading to significant spatiotemporal heterogeneity in actual water

environments [5,6]. Epidemiological and toxicological studies have associated long-term DBPs exposure with increased risks of bladder cancer, colorectal cancer, and reproductive toxicity [1,2]. Notably, mixed exposure to multiple DBPs may produce synergistic, antagonistic, or additive effects, increasing the complexity of health risk assessment [7].

1.2. Current status and challenges in DBPs toxicity research

DBPs toxicity research faces several key challenges. Traditional studies have focused on single exposure to a few regulated DBPs, while research on combined toxic effects of complex DBPs mixtures remains scarce. Wei et al. demonstrated that structurally similar haloacetonitrile DBPs may produce significant additive toxic effects, emphasizing the need for mixture-based risk assessment [8]. Additionally, conventional toxicity detection typically requires high concentrations, potentially underestimating effects at environmentally relevant levels [9]. Current monitoring systems only test a few regulated DBPs, unable to comprehensively reflect true pollution situations. Liu et al.'s study of the Taihu Lake drinking water system showed that DBPs distribution exhibits distinct seasonal and regional characteristics [10], while Yu et al. demonstrated that machine learning methods could effectively analyze distribution patterns and health risks of haloacetic acids in water distribution systems [6]. Another significant challenge is extrapolating in vitro findings to human health impacts. Kalita et al. highlighted the need to integrate multi-level biological responses to construct a causal chain from molecular events to health outcomes [2], emphasizing the importance of identifying new biomarkers that reflect early cellular functional changes.

1.3. Cellular biomechanical parameters as a new perspective for toxicity evaluation

Cellular biomechanical properties, including elasticity, viscoelasticity, deformability, and tension, are sensitive indicators of cellular responses to environmental changes [11]. With advances in atomic force microscopy (AFM), microfluidic analysis, and high-throughput deformation techniques, quantitative measurement of these properties has become important for exploring cellular function [12–14]. Darling and Di Carlo noted that biomechanical changes often precede biochemical changes and can serve as early indicators of cellular status [12]. These properties are closely related to pathological states—cancer cells exhibit decreased elasticity and enhanced deformability related to their invasive capabilities, while cardiovascular and neurodegenerative diseases show significant changes in specific cell types' biomechanical properties. Environmental toxicants can affect these properties through multiple mechanisms, including cytoskeletal protein interference and membrane fluidity alterations [15–17]. Wang et al. first reported that 2,6-dichloro-1,4-benzoquinone, a novel DBP, can cause immune cell dysfunction potentially related to membrane integrity and cytoskeletal disruption [18]. However, systematic research on different DBPs' effects on cellular biomechanics remains largely unexplored.

1.4. Research objectives and innovations

This study aims to integrate water quality monitoring data analysis with cellular biomechanics research to explore correlations between DBPs pollution patterns and cellular biomechanical effects. Specific objectives include: (1) identifying typical DBPs pollution patterns from water quality monitoring data; (2) studying representative DBPs' effects on cell membrane properties, cytoskeletal structure, and cell adhesion; (3) analyzing dose-effect relationships between different DBPs patterns and biomechanical effects; and (4) exploring the feasibility of biomechanical parameters as new indicators for DBPs toxicity.

Figure 1 presents a schematic overview of the integrated approach used in this study. The workflow consists of three main components: (1) data collection and preprocessing from 12 water treatment plants, resulting in a comprehensive dataset of 5184 samples with 18 DBPs compounds; (2) pattern recognition and classification using PCA and cluster analysis, which identified four distinct DBPs pollution patterns with characteristic compositions; and (3) multi-parametric biomechanical analysis using AFM, microfluidic deformation testing, and cytoskeletal structure evaluation to assess the cellular impacts of these patterns. This integrated approach bridges environmental monitoring with cellular biomechanics to establish relationships between DBPs pollution patterns and their potential health effects.

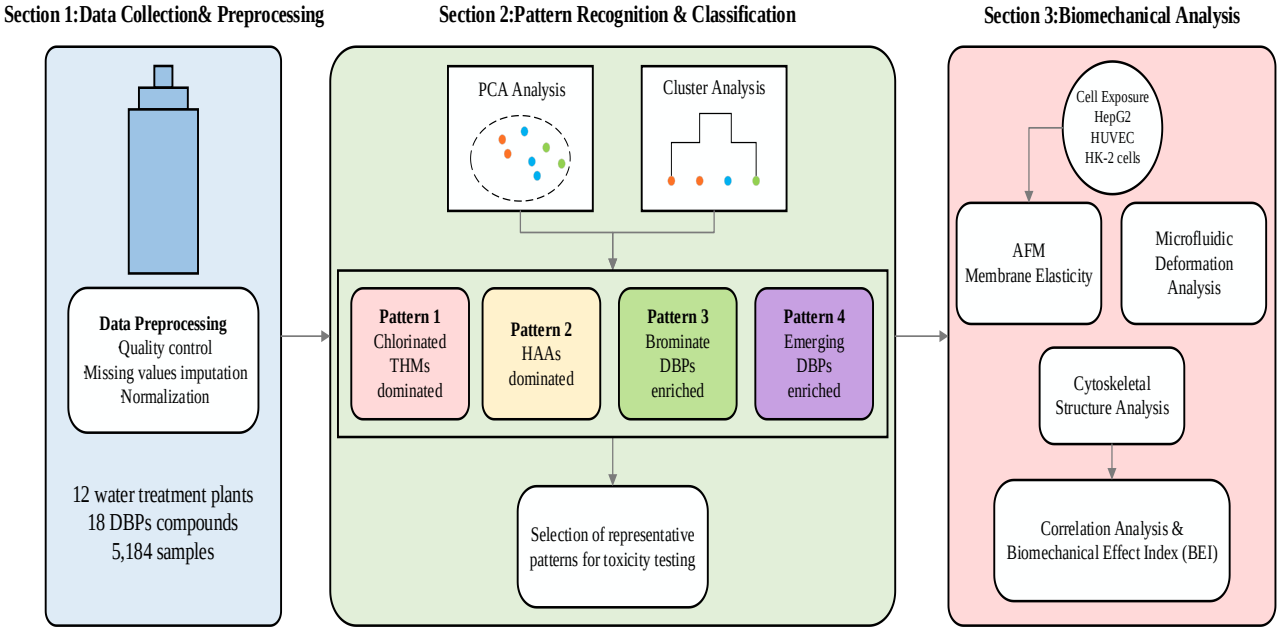

Figure 1. Workflow of the integrated approach for DBPs pattern recognition and biomechanical analysis.

The innovations include: integrating data-driven pollution pattern recognition with molecular toxicology; systematically studying DBPs effects on cellular biomechanics; establishing association models between pollution patterns and biomechanical effects; and proposing new approaches for DBPs toxicity screening based on biomechanical parameters. This research aims to enhance understanding of DBPs health risks while opening new directions for interdisciplinary research between environmental toxicology and biomechanics.

2. Research materials and methods

2.1. Water quality monitoring data acquisition and preprocessing

Drinking water quality monitoring data were collected from 12 water treatment plants and their distribution networks across three metropolitan areas in Eastern China from January 2022 to December 2024. The monitoring program included 8 regulated DBPs (4 THMs, 4 HAAs) and 10 unregulated emerging DBPs (3 haloketones, 3 haloacetonitriles, 2 halobenzoquinones, 2 haloacetamides). Samples were collected monthly, resulting in 5184 samples with complete DBPs concentration profiles. The selection of these 18 specific DBPs was based on several criteria: (1) inclusion of regulated DBPs (THMs and HAAs) that are routinely monitored and have established health risk assessments; (2) representation of major structural classes including carbon-halogen (THMs), carboxylic acid (HAAs), nitrile (HANs), and aromatic (HBQs) compounds; (3) coverage of both chlorinated and brominated species to assess the impact of halogen type; (4) inclusion of emerging DBPs identified as high-priority based on previous toxicity and occurrence studies [3,4,18]; and (5) analytical feasibility for consistent detection at environmentally relevant concentrations. While over 700 DBPs have been identified in drinking water systems [2], these 18 compounds were selected to provide a representative and analytically feasible subset that captures the diversity of chemical structures, formation pathways, and potential toxicity mechanisms, while focusing on species most frequently detected in the studied water systems based on preliminary screening.

Relevant water quality parameters were monitored simultaneously, including temperature, pH, turbidity, residual chlorine, dissolved organic carbon (DOC), UV254 absorbance, bromide concentration, and ammonia nitrogen. **Table 1** presents the key water quality parameters and DBPs concentrations in the dataset.

Table 1. Summary of key water quality parameters and DBPs concentrations in the monitoring dataset.

Category	Parameter	Mean ± SD	Detection frequency (%)
Water Quality	Temperature (°C)	18.5 ± 7.8	100
	pH	7.35 ± 0.41	100
	DOC (mg/L)	2.75 ± 1.15	100
	Bromide (μg/L)	42.5 ± 52.8	96.3
Regulated DBPs	Chloroform (μg/L)	18.7 ± 12.5	99.8
	Dichloroacetic acid (μg/L)	15.8 ± 8.9	99.5
Emerging DBPs	Dichloroacetonitrile (μg/L)	2.4 ± 2.1	82.5
	2,6-Dichloro-1,4-benzoquinone (μg/L)	0.15 ± 0.22	48.5

Prior to analysis, all data underwent quality control and preprocessing. Missing values (< 3%) were imputed using the *k*-nearest neighbor algorithm. Outliers were identified using the modified *Z*-score method and validated through quality assurance records. Measurements below detection limits were replaced with half of the detection limit [10]. All parameters were normalized using min-max scaling.

2.2. DBPs pollution pattern recognition and data mining

Multiple approaches were employed to identify distinct DBPs pollution patterns. Principal component analysis (PCA) was applied to reduce dimensionality and identify main factors explaining variance in DBPs concentrations. The Kaiser criterion (eigenvalues > 1) determined optimal principal components. Factor loadings identified individual DBPs contributions to each principal component.

Cluster analysis, using both hierarchical (Ward's method with Euclidean distance) and *k*-means clustering, identified distinct patterns. Optimal cluster numbers were determined using silhouette coefficient analysis and the elbow method. Self-organizing maps (SOMs) and random forest classification further enhanced pattern recognition and explored non-linear relationships between DBPs and water quality parameters. Model performance was evaluated using 10-fold cross-validation.

Based on pattern recognition results, four distinct pollution patterns were identified for cellular biomechanical effect studies, as shown in **Table 2**.

Table 2. Characteristics of typical DBPs pollution patterns selected for cellular biomechanical effect studies.

Characteristic	Pattern 1 (Chlorinated THMs dominated)	Pattern 2 (HAAs dominated)	Pattern 3 (Brominated DBPs enriched)	Pattern 4 (Emerging DBPs enriched)
Total DBPs concentration	Moderate (45–60 μg/L)	High (65–85 μg/L)	Moderate (40–55 μg/L)	Low to moderate (35–50 μg/L)
Dominant DBPs class	THMs (> 60% of total)	HAAs (> 55% of total)	Mixed (40%–45% THMs, 35%–40% HAAs)	Mixed (35%–40% THMs, 30%–35% HAAs)
Brominated species	Low (< 20% of total THMs)	Moderate (25%–35% of total HAAs)	High (> 50% of total DBPs)	Moderate (30%–40% of total DBPs)
Emerging unregulated DBPs	Low (< 5% of total)	Low to moderate (5%–10% of total)	Moderate (10%–15% of total)	High (> 20% of total)

For each pollution pattern, both synthetic DBPs mixtures (prepared according to the typical composition profile) and actual water samples (collected from representative water sources) were selected for cellular exposure experiments. The synthetic mixtures were prepared using analytical-grade standards of individual DBPs diluted in ultrapure water and adjusted to match typical water quality parameters (pH, ionic strength) of drinking water. Actual water samples were collected, transported, and stored according to standard protocols to minimize changes in DBPs concentrations before the experiments [9].

2.3. Cell models and exposure protocol

Three human cell lines were selected: HepG2 (human hepatocellular carcinoma) representing liver cells, HUVEC (human umbilical vein endothelial cells) representing vascular endothelial cells, and HK-2 (human kidney proximal tubule cells) representing kidney epithelial cells. These were selected based on their relevance to DBPs metabolism, distribution, and potential toxicity targets [2,7,9].

Cells were cultured in appropriate media with supplements at 37 °C in a humidified atmosphere with 5% CO_2. For exposure experiments, cells at 70%–80% confluence were exposed to synthetic DBPs mixtures or actual water samples in serum-free media. **Table 3** summarizes the exposure conditions.

Table 3. Key exposure concentrations of DBPs mixtures and actual water samples.

Exposure group	Concentration level	Total DBPs (μg/L)	Fold of environmental level	Cell viability (% of control)
Synthetic mixtures	Environmental	40–75 (pattern-dependent)	1×	> 90%
	Medium	400–750	10×	60%–80%
	High	1200–2250	30×	40%–65%
Actual water samples	Environmental	35–85 (pattern-dependent)	1×	> 90%
	Concentrated	350–850	10×	55%–80%

Exposure durations were set at 24 h, 48 h, and 72 h to evaluate both acute and sub-chronic effects. Cell viability was assessed using the MTT assay to ensure sub-lethal exposure concentrations, as cytotoxicity could confound biomechanical changes interpretation.

2.4. Measurement of cellular biomechanical properties

A multiparametric approach was employed to comprehensively characterize the biomechanical properties of cells exposed to different DBPs pollution patterns. Three complementary techniques were used: atomic force microscopy (AFM) for high-resolution assessment of cell membrane elasticity, microfluidic cell deformation analysis for whole-cell deformability measurement, and traction force microscopy for cell-substrate interaction evaluation.

2.4.1. Atomic force microscopy (AFM) measurements

Cellular elastic properties were quantified using a Bruker Dimension Icon AFM system. Silicon nitride cantilevers (spring constant 0.06 N/m) with pyramidal tips were used. Force-distance curves were acquired at multiple locations on each cell with an approach velocity of 2 μm/s and a maximum indentation force of 1 nN. For each condition, at least 30 cells were analyzed with 10 force curves per cell. Young's modulus was calculated by fitting force-distance curves to the Hertz model.

Force-volume mapping generated elasticity maps (32 × 32 resolution over 20 × 20 μm areas) to assess mechanical heterogeneity within cells. Mean elasticity, standard deviation, and skewness of elasticity distribution were extracted.

2.4.2. Microfluidic cell deformation analysis

Whole-cell deformability was assessed using a custom microfluidic device with constriction channels (8 μm width, 15 μm height, 50 μm length). Cell suspensions were driven through microchannels at 15 kPa pressure. Cell deformation was recorded at 2000 frames per second and analyzed to extract: entry time, transit velocity, deformation index, and recovery ratio.

Statistical analysis of microfluidic deformation data was performed using a two-step approach. First, the Kolmogorov-Smirnov test was applied to determine if the deformation parameters (entry time, transit velocity, deformation index, and recovery ratio) followed a normal distribution. For normally distributed parameters, one-way ANOVA followed by Dunnett's post-hoc test was used to compare treated groups with control. For non-normally distributed parameters, the Kruskal-Wallis test followed by Dunn's post-hoc test was employed. Statistical significance was established at $p < 0.05$. To ensure data reliability, outliers beyond three standard deviations from the mean

were excluded, and the coefficient of variation was calculated across experimental replicates to verify measurement consistency. All microfluidic experiments were performed at least three times with a minimum of 200 cells analyzed per condition, providing robust statistical power for detecting significant differences between treatment groups.

2.4.3 Cytoskeletal structure analysis

Immunofluorescence staining and confocal microscopy correlated biomechanical changes with cytoskeletal alterations. F-actin was stained with Alexa Fluor 488-phalloidin, microtubules with anti-α-tubulin antibody, and nuclei with DAPI. Confocal *z*-stack images were acquired using a Leica SP8 microscope. ImageJ software quantified cytoskeletal parameters including F-actin intensity, microtubule network density, focal adhesion size/distribution, and nuclear morphology.

2.5. Statistical analysis and model construction

All measurements were performed in at least three independent experiments. Data normality was assessed using the Shapiro-Wilk test. For normally distributed data, one-way ANOVA with Tukey's post-hoc test compared multiple groups. For non-normally distributed data, the Kruskal-Wallis test with Dunn's post-hoc test was applied. Dose-response relationships were analyzed using regression analysis. Principal component analysis identified main modes of variation in biomechanical responses. Canonical correlation analysis identified associations between DBPs features and biomechanical responses. Partial least squares regression models predicted biomechanical responses from DBPs profiles, evaluated using cross-validation. A Biomechanical Effect Index (BEI) was developed as a weighted sum of normalized changes in key biomechanical parameters. Weights were determined based on parameter reliability and sensitivity through repeatability tests and dose-response analyses. BEI values ranked the effects of different DBPs patterns and explored correlations with conventional toxicity endpoints.

3. Research results

3.1. DBPs pollution characteristics and patterns in water quality monitoring data

Analysis of the water quality monitoring dataset revealed distinct spatiotemporal patterns in DBPs occurrence. Principal component analysis identified four principal components explaining 78.6% of the total variance in DBPs concentrations. As shown in **Figure 2**, the first two principal components (PC1 and PC2) explained 42.3% and 18.7% of the variance, respectively. PC1 was associated with chlorinated THMs and HAAs, while PC2 related primarily to brominated DBPs species.

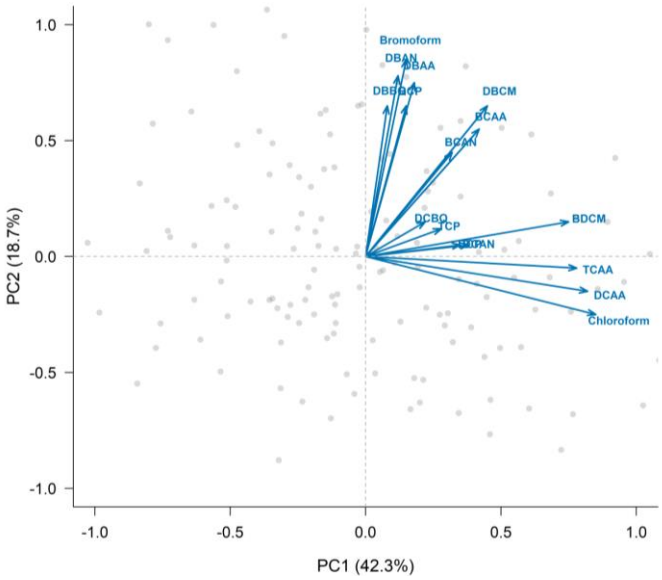

Figure 2. PCA biplot of DBPs species.

Figure 2 showed the distribution of DBPs species and samples in the first two principal component spaces. Different DBPs species are represented by blue arrows, while individual water samples are shown as grey dots. The direction and length of the arrows indicate the contribution of each DBPs species to the principal components.

Cluster analysis identified four distinct pollution patterns, each with characteristic DBPs composition and water quality associations. As shown in **Table 4**, Pattern 1 (Chlorinated THMs dominated) featured high concentrations of chloroform and dichloroacetic acid with relatively low brominated species. Pattern 2 (HAAs dominated) showed elevated levels of di- and trichloroacetic acids. Pattern 3 (Brominated DBPs enriched) exhibited a high proportion of brominated species. Pattern 4 (Emerging DBPs enriched) was distinguished by elevated concentrations of unregulated DBPs.

Table 4. Mean concentrations (μg/L) of key DBPs in the four identified pollution patterns.

DBPs	Pattern 1	Pattern 2	Pattern 3	Pattern 4
Chloroform	28.5 ± 6.2	15.8 ± 4.5	8.4 ± 3.2	12.6 ± 4.1
Bromodichloromethane	10.2 ± 3.5	8.6 ± 2.8	12.5 ± 3.6	9.8 ± 3.2
Dichloroacetic acid	10.6 ± 3.2	22.4 ± 5.3	7.2 ± 2.5	8.4 ± 2.8
Bromochloroacetic acid	3.2 ± 1.5	6.8 ± 2.4	10.5 ± 3.4	5.8 ± 2.2
2,6-Dichloro-1,4-benzoquinone	0.05 ± 0.02	0.08 ± 0.04	0.06 ± 0.03	0.42 ± 0.18
Total regulated DBPs	68.0 ± 12.5	79.1 ± 15.2	76.3 ± 14.8	55.7 ± 11.2
Total emerging DBPs	3.6 ± 1.4	5.5 ± 2.2	5.4 ± 2.1	11.3 ± 3.5
Brominated/total ratio	0.17 ± 0.05	0.21 ± 0.06	0.58 ± 0.12	0.33 ± 0.08

The temporal distribution of these patterns exhibited distinct seasonal trends. Pattern 1 showed winter dominance, Pattern 2 demonstrated summer prevalence, Pattern 3 exhibited less pronounced seasonal variation, and Pattern 4 showed bimodal distribution with peaks in spring and autumn. Random forest analysis identified

temperature and DOC as key factors for Pattern 2, while bromide concentration strongly predicted Pattern 3. Pattern 4 was associated with pH and residual chlorine levels.

3.2. Cytoskeletal and mechanical alterations induced by DBPs exposure

DBPs exposure induced significant changes in both cellular mechanical properties and cytoskeletal organization across all cell types. Atomic force microscopy (AFM) measurements revealed concentration-dependent increases in Young's modulus (stiffening) of cells following exposure to DBPs, with Pattern 4 (Emerging DBPs enriched) inducing the most pronounced effect. As shown in **Figure 3**, Pattern 4 caused a 5.4-fold increase in Young's modulus of HepG2 cells at the highest concentration, followed by Pattern 3 (4.5-fold), Pattern 2 (3.9-fold), and Pattern 1 (3.0-fold). At environmentally relevant concentrations, only Pattern 4 induced statistically significant stiffening (1.4-fold increase, $p < 0.05$).

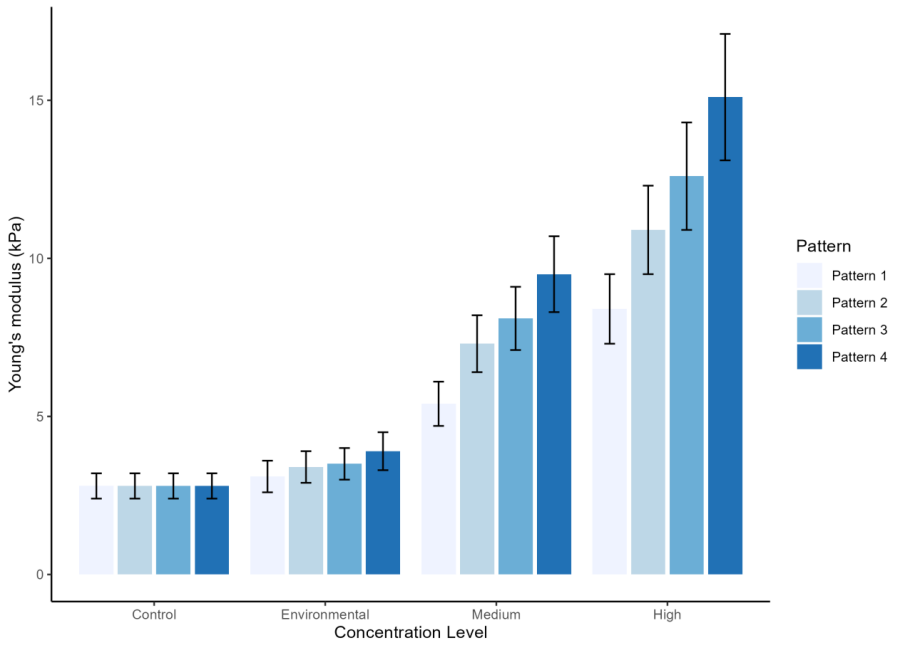

Figure 3. Changes in Young's modulus of HepG2 cells after DBPs exposure (Error bars represent standard deviation from measurements of at least 30 cells with 10 force curves per cell).

The elasticity changes varied among cell types, with HK-2 cells showing the highest sensitivity to DBPs-induced stiffening, followed by HepG2 and HUVEC cells. **Table 5** compares the fold changes in Young's modulus across different cell types after exposure to environmental and medium concentration levels of each DBPs pattern.

Table 5. Fold changes in Young's modulus of different cell types after 48-h exposure to DBPs.

Cell Type	Concentration	Pattern 1	Pattern 2	Pattern 3	Pattern 4
HepG2	Environmental	1.12 ± 0.10	1.20 ± 0.12	1.24 ± 0.15	1.40 ± 0.18*
	Medium	1.92 ± 0.25*	2.60 ± 0.32**	2.88 ± 0.38**	3.40 ± 0.45***
HUVEC	Environmental	1.08 ± 0.09	1.15 ± 0.11	1.18 ± 0.12	1.25 ± 0.14
	Medium	1.65 ± 0.22*	2.10 ± 0.28*	2.45 ± 0.32**	2.85 ± 0.38**
HK-2	Environmental	1.18 ± 0.12	1.28 ± 0.15	1.35 ± 0.16*	1.52 ± 0.20*
	Medium	2.15 ± 0.28*	2.85 ± 0.35**	3.25 ± 0.42***	3.80 ± 0.50***

Values represent fold change relative to control cells (mean ± SD). Asterisks indicate statistical significance compared to control (*$p < 0.05$, **$p < 0.01$, ***$p < 0.001$).

AFM force-volume mapping revealed changes not only in mean elasticity but also in the spatial distribution of mechanical properties across the cell surface. Control cells showed relatively homogeneous elasticity maps with slight variations between the cell center and periphery. In contrast, DBPs-exposed cells exhibited increased mechanical heterogeneity, particularly in Pattern 3 and Pattern 4 exposures, where distinct stiff regions were observed, often coinciding with altered cytoskeletal structure.

Confocal microscopy revealed significant reorganization of F-actin and microtubule networks following DBPs exposure. Control HepG2 cells showed predominantly cortical actin organization with few stress fibers, while cells exposed to DBPs exhibited concentration-dependent increases in stress fiber formation, with Pattern 4 inducing the most pronounced effect. Quantitative analysis confirmed these observations across all cytoskeletal parameters (**Table 6**).

Table 6. Quantitative analysis of cytoskeletal parameters in HepG2 cells after 48-h exposure to DBPs at medium concentration level.

Cytoskeletal Parameter	Control	Pattern 1	Pattern 2	Pattern 3	Pattern 4
F-actin intensity (fold change)	1.00 ± 0.08	1.65 ± 0.18*	1.85 ± 0.22**	2.05 ± 0.25**	2.35 ± 0.28***
Stress fiber content (% of total actin)	18.5 ± 3.2	38.6 ± 4.5*	45.2 ± 5.2**	42.8 ± 4.8**	48.5 ± 5.5***
Cortical actin thickness (μm)	0.68 ± 0.12	0.92 ± 0.15	0.85 ± 0.14	0.75 ± 0.13	0.62 ± 0.11
Microtubule network density (%)	100.0 ± 8.5	85.2 ± 7.8	78.5 ± 7.2*	72.6 ± 6.5*	68.4 ± 6.2**
Focal adhesion size (μm²)	1.25 ± 0.18	1.85 ± 0.24*	2.12 ± 0.28**	2.25 ± 0.30**	2.45 ± 0.32**
Focal adhesion number (per cell)	28.5 ± 4.2	35.8 ± 5.1	38.5 ± 5.5*	32.6 ± 4.8	30.5 ± 4.5
Nuclear area (μm^2)	185.2 ± 15.6	175.6 ± 14.8	168.5 ± 13.5	162.4 ± 13.2*	158.6 ± 12.8*

Note: Values are presented as mean ± SD. Asterisks indicate statistical significance compared to control (*$p < 0.05$, **$p < 0.01$, ***$p < 0.001$).

All DBPs patterns induced significant changes in F-actin intensity, stress fiber formation, and microtubule network density in a concentration-dependent manner. Pattern 4 exhibited the strongest effects, with a 2.8-fold increase in stress fiber content and a 45% decrease in microtubule network density at the highest concentration. Time-dependent analysis revealed that short-term exposure (24 h) primarily induced stress fiber formation without significant disorganization, suggesting an initial adaptive response. Prolonged exposure (72 h) led to increased cytoskeletal disorganization,

particularly in Pattern 3 and Pattern 4 exposures, indicating potential cytoskeletal breakdown after initial adaptation failure.

These integrated findings suggest a mechanistic link between DBPs exposure, cytoskeletal reorganization, and alterations in cellular mechanical properties, with the cytoskeletal changes likely underpinning the observed mechanical effects. The pattern-specific responses, particularly the pronounced effects of Patterns 3 and 4, indicate that brominated and emerging DBPs may disrupt cellular mechanics through pathways distinct from those affected by chlorinated species.

3.3. Effects of DBPs exposure on cell adhesion and migration abilities

Microfluidic deformation analysis revealed significant changes in whole-cell deformability following DBPs exposure. As shown in **Figure 4**, cells exposed to all four DBPs patterns exhibited reduced deformability (longer entry times and lower deformation indices) in a concentration-dependent manner.

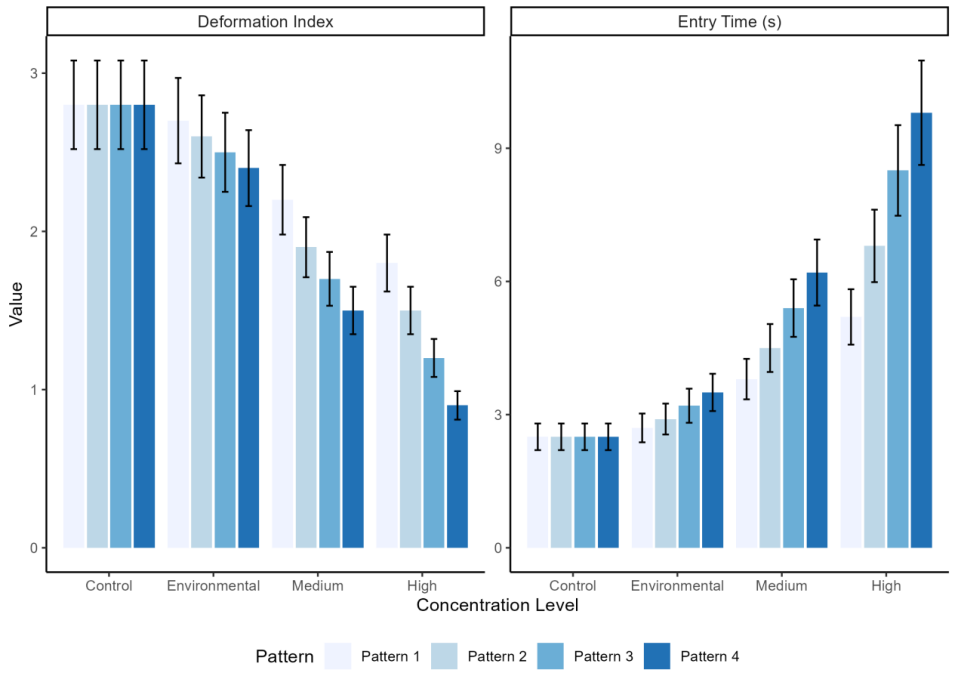

Figure 4. Effects of DBPs exposure on cell deformability parameters: **(A)** Deformation index—lower values indicate decreased deformability; **(B)** Entry time—longer times indicate decreased deformability (Error bars represent standard deviation from analysis of at least 200 cells per condition).

As shown in **Figure 4**, Pattern 3 and Pattern 4 induced the most pronounced effects on cellular deformability. Cells exposed to Pattern 4 at high concentration exhibited a 3.9-fold increase in entry time compared to control, while Pattern 3 caused a 3.4-fold increase. The deformation index decreased most significantly in Pattern 4 (47% reduction) and Pattern 3 (39% reduction). The observed changes correlated strongly with cytoskeletal alterations, suggesting a mechanistic link between DBPs-induced cytoskeletal reorganization and impaired mechanical function.

Cell recovery analysis provided further insights into the viscoelastic properties of exposed cells. Control cells exhibited nearly complete shape recovery (ratio of 0.95),

while cells exposed to DBPs showed significantly impaired recovery in a pattern- and concentration-dependent manner. Pattern 4 exposure resulted in the most severe impairment (recovery ratio of 0.52 at high concentration), indicating substantial permanent deformation.

Cell migration analysis revealed that all DBPs patterns induced concentration-dependent decreases in migration capability. Cells exposed to Pattern 4 at high concentration showed an 82% reduction in migration distance, while Pattern 3, Pattern 2, and Pattern 1 exposures led to 70%, 57%, and 45% reductions, respectively. These effects correlated with changes in focal adhesion properties, suggesting that altered cell-substrate interactions contribute to reduced migration capacity.

3.4. Correlation between different pollution patterns and cellular biomechanical effects

Canonical correlation analysis revealed systematic relationships between DBPs composition and biomechanical parameters. As shown in **Figure 5**, the first canonical variate (explaining 68.5% of shared variance) revealed strong positive correlations between chlorinated DBPs and cellular stiffening parameters while showing negative correlations with deformation index and migration distance.

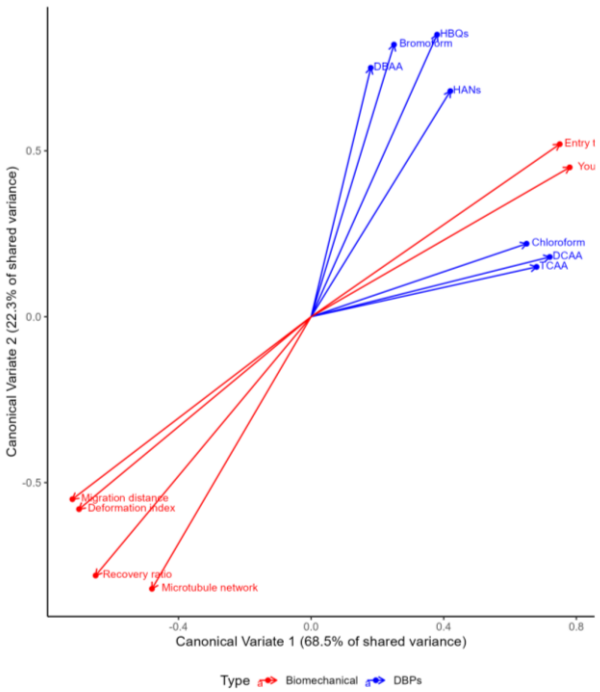

Figure 5. Canonical correlation analysis between DBPs characteristics and cellular biomechanical parameters.

Arrow length indicates loading strength, and proximity between arrows indicates correlation strength. As illustrated in **Figure 5**, the second canonical variate (explaining 22.3% of shared variance) highlighted strong associations between brominated/emerging DBPs and disruptions in microtubule network density and recovery ratio, suggesting they may affect cellular mechanics through different mechanisms than chlorinated DBPs.

Based on comprehensive assessments, a composite Biomechanical Effect Index

(BEI) was calculated for each DBPs pattern. Pattern 4 consistently exhibited the highest BEI values across all concentration levels, reaching the "Severe Effect" threshold at medium and high concentrations. Pattern 3 showed the second strongest effects, while Patterns 2 and 1 showed progressively lower BEI values. At environmentally relevant concentrations, only Pattern 4 exceeded the "Low Effect" threshold (BEI = 0.35), indicating that emerging unregulated DBPs may pose biomechanical alteration risks even at typical drinking water concentrations.

To further validate the biological relevance of the BEI as an early indicator of DBPs toxicity, we conducted correlation analyses between BEI values and traditional cytotoxicity endpoints across all four DBPs patterns. Strong negative correlations were observed between BEI values and IC50 values for cell viability ($r = -0.85$, $p < 0.001$) and GSH depletion ($r = -0.82$, $p < 0.001$). Importantly, when comparing concentration-response relationships, significant biomechanical alterations (BEI > 0.35) were detectable at concentrations 3–5 times lower than those required for observable cytotoxicity (≥ 20% reduction in cell viability). This enhanced sensitivity was particularly evident for Pattern 4 (Emerging DBPs enriched), where BEI reached the 'Low Effect' threshold at environmentally relevant concentrations that showed no detectable impact on conventional endpoints. These findings highlight the unique value of BEI as an early warning indicator capable of detecting subtle cellular alterations before overt cytotoxicity occurs, potentially addressing a critical gap in current risk assessment approaches that rely primarily on apical toxicity endpoints.

4. Discussion

4.1. Methodological value and application prospects of DBPs pollution pattern recognition

The pattern recognition approach employed in this study represents a significant advancement in understanding DBPs occurrence in drinking water systems. By analyzing the extensive monitoring dataset comprising 5184 samples from 12 water treatment plants across three metropolitan areas, we successfully identified four distinct pollution patterns with characteristic DBPs compositions and water quality associations. This data-driven methodology overcomes several limitations of traditional DBPs monitoring approaches. Conventional monitoring typically focuses on a few regulated DBPs without considering their complex interrelationships or co-occurrence patterns, potentially underestimating the true exposure risks. Our approach provides a more comprehensive understanding of DBPs pollution by capturing the heterogeneous nature of DBPs mixtures in real drinking water systems.

The identified patterns demonstrate clear associations with water quality parameters and seasonal variations, suggesting that predictive models could be developed to anticipate DBPs profile changes based on source water characteristics and treatment conditions. Pattern 1 (Chlorinated THMs dominated) showed strong winter dominance, likely due to increased chlorine dosage and reduced natural organic matter biodegradation during colder months. Pattern 2 (HAAs dominated) exhibited summer prevalence, consistent with previous studies showing enhanced HAA formation under higher temperature conditions that accelerate oxidation reactions

between chlorine and organic precursors. The less pronounced seasonal variation of Pattern 3 (Brominated DBPs enriched) reflects its stronger dependence on bromide concentration in source water rather than seasonal factors, as confirmed by our random forest analysis. The bimodal distribution of Pattern 4 (Emerging DBPs enriched) with peaks in spring and autumn suggests complex formation mechanisms potentially related to seasonal changes in organic matter composition during periods of ecological transition.

The pattern recognition methodology demonstrates significant potential for integration into intelligent water quality monitoring systems. By identifying characteristic DBPs profiles associated with specific water quality conditions, utilities could implement targeted monitoring strategies focused on representative DBPs for each pattern rather than conducting comprehensive analysis for all compounds. This would enable more cost-effective monitoring while maintaining comprehensive risk assessment capabilities. Furthermore, the established relationships between water quality parameters and DBPs patterns could facilitate the development of early warning systems to predict potential shifts in DBPs profiles based on changes in key water quality indicators such as temperature, dissolved organic carbon, and bromide concentration.

Beyond monitoring applications, this methodology provides valuable insights for water treatment optimization. Each identified pattern corresponds to different formation mechanisms and precursor relationships, suggesting pattern-specific treatment strategies. For instance, Pattern 2 (HAAs dominated) showed strong associations with dissolved organic carbon, indicating that enhanced coagulation and granular activated carbon filtration might be particularly effective for reducing this pattern's occurrence. Similarly, Pattern 3 (Brominated DBPs enriched) could potentially be mitigated through ion exchange processes targeting bromide removal from source water. These targeted approaches represent more efficient utilization of treatment resources compared to general strategies that may not address the specific characteristics of local DBPs profiles.

4.2. Cellular biomechanical changes as sensitive indicators for DBPs toxicity evaluation

Our investigation into cellular biomechanical responses to DBPs exposure reveals a promising new dimension for toxicity assessment. The multiparametric approach combining atomic force microscopy, microfluidic deformation analysis, and cytoskeletal structure evaluation provided comprehensive insights into how different DBPs patterns affect cellular mechanical properties. These biomechanical alterations demonstrated both sensitivity and pattern specificity, suggesting their potential utility as early indicators of DBPs-induced cellular dysfunction.

The exceptional sensitivity of biomechanical parameters to DBPs exposure was particularly evident for Pattern 3 (Brominated DBPs enriched) and Pattern 4 (Emerging DBPs enriched). Significant changes in Young's modulus and cytoskeletal organization were detectable at concentrations 5–10 times lower than those required for conventional cytotoxicity. This enhanced sensitivity was most pronounced in HK-2 kidney cells, which exhibited significant stiffening (1.52-fold increase in Young's

modulus) even at environmentally relevant concentrations of Pattern 4, addressing a critical gap in current risk assessment approaches that rely primarily on high-dose toxicity endpoints.

Pattern-specific biomechanical responses provided insights into potential mechanisms of DBPs toxicity. Pattern 4, dominated by emerging unregulated DBPs, consistently induced the most profound alterations across all cell types and parameters. The strong effects observed with Pattern 3 support the growing concern that brominated DBPs may pose greater health risks than their chlorinated counterparts [19]. Canonical correlation analysis revealed that brominated and emerging DBPs were strongly associated with disruptions in microtubule network density and cellular recovery capacity, while chlorinated DBPs showed stronger correlations with cellular stiffening.

Compared to traditional toxicity endpoints, biomechanical parameters offer several advantages: higher sensitivity at environmentally relevant concentrations, mechanistic insights linking specific alterations to cytoskeletal disruptions, and integration potential through the composite Biomechanical Effect Index (BEI). The strong correlations between BEI values and established toxicity measures ($r = -0.85$ with IC50 for cell viability and $r = -0.82$ with GSH depletion) validate the biological relevance of these alterations as potential surrogate markers for more complex toxicological endpoints.

The application potential extends to practical DBPs screening applications, where high-throughput deformation analysis combined with AFM measurements could enable rapid screening of water samples without extensive chemical characterization, particularly valuable for identifying emerging concerns not yet included in standard monitoring protocols.

4.3. Bridging mechanisms from cellular biomechanical changes to human health risks

The translation of cellular biomechanical alterations to potential human health impacts represents both a challenge and an opportunity in environmental health research. Our findings establish a foundation by demonstrating consistent relationships between DBPs exposure, cellular mechanical dysfunction, and established toxicity endpoints. The observed cytoskeletal reorganization provides mechanistic insight into how DBPs disrupt cellular function at the molecular level, with strong correlations between stress fiber content and cellular stiffening, and between microtubule disruption and impaired deformability.

These biomechanical alterations may extend to tissue-level dysfunction through several mechanisms. In vascular endothelial cells (HUVEC), the observed stiffening and reduced migration capacity could impact vascular integrity and repair mechanisms critical for cardiovascular health. Endothelial cell stiffening is associated with reduced nitric oxide production and impaired vasodilation, potentially contributing to cardiovascular disorders. Similarly, the pronounced effects in HK-2 kidney cells suggest implications for renal function, as cellular mechanical properties play crucial roles in kidney functions. The high sensitivity of HK-2 cells to DBPs-induced biomechanical alterations aligns with epidemiological evidence linking long-term

DBPs exposure to kidney and bladder cancer risks.

Pattern-specific responses further support connections between cellular mechanical alterations and disease processes. Pattern 4 (Emerging DBPs enriched) strongly affected cytoskeletal integrity and recovery capacity, consistent with emerging DBPs causing oxidative stress and protein modification that impact cytoskeletal proteins [20]. Wang et al.'s finding that 2,6-dichloro-1,4-benzoquinone induces immune cell dysfunction related to membrane integrity and cytoskeletal disruption supports this mechanism [21]. Similarly, Pattern 3's effects on microtubule network density suggest interference with microtubule dynamics, potentially impacting cellular division and structural integrity.

The development of risk assessment models based on biomechanical parameters represents a promising research direction. The strong correlations between our Biomechanical Effect Index and established toxicity measures suggest that integrated biomechanical assessments could serve as reliable indicators of cellular health status. Establishing dose-response relationships could enable predictive models that estimate tissue-specific effects based on water quality data, accounting for the complex interplay between different DBPs. Our canonical correlation analysis represents an initial step toward such integrative modeling, identifying specific relationships that could form the basis for more sophisticated predictive frameworks.

4.4. Research limitations and future research directions

Despite the insights gained, important methodological limitations exist. The in vitro cell models used cannot fully recapitulate the complex in vivo environment with its three-dimensional architecture and intercellular interactions. This limitation is particularly relevant when extrapolating to long-term, low-dose exposure scenarios typical of human DBPs exposure. Future studies should explore advanced tissue models, organoids, or co-culture systems that better simulate physiological complexity and provide more translatable insights into DBPs toxicity mechanisms.

The statistical approaches employed, while powerful for high-dimensional data analysis, have inherent limitations. PCA assumes linear relationships and can be sensitive to outliers, while clustering results depend on methodological choices. To address these limitations, we employed multiple complementary approaches and cross-validation. Future work could incorporate non-linear dimensionality reduction techniques (*t*-SNE, UMAP) and ensemble methods to capture more complex data relationships and further validate the identified patterns.

Additionally, our study included only 18 representative DBPs, a small fraction of the more than 700 DBPs identified in drinking water. The synthetic mixtures, though designed to match identified pollution patterns, may not capture all biologically active components present in actual drinking water. The extrapolation from cellular models to human health impacts remains challenging. The concentrations required to induce significant biomechanical changes for Patterns 1 and 2 were higher than typical environmental levels, raising questions about real-world relevance. However, the significant effects observed with Pattern 4 at environmentally relevant concentrations suggest that emerging DBPs may pose risks warranting further investigation.

Future research should address these limitations through: (1) Long-term, low-

dose exposure studies to better simulate chronic human exposure conditions; (2) advanced three-dimensional tissue models or organoids for more physiologically relevant assessments; and (3) in vivo validation studies to confirm relationships between cellular biomechanical alterations and tissue-level dysfunction.

Technological advancements should focus on developing high-throughput biomechanical screening platforms and integrating these measurements with other biomarkers (genomic, proteomic, metabolomic) for a comprehensive understanding of toxicity mechanisms. Machine learning approaches could identify patterns not apparent through conventional analyses.

Ultimately, epidemiological studies incorporating biomechanical biomarkers could bridge the gap between laboratory findings and human health impacts. Blood cell-based biomechanical assays applied in population studies could help identify early indicators of DBPs exposure effects and correlate these with specific health outcomes, advancing our understanding of DBPs health risks and informing more effective water safety management strategies.

5. Conclusion

This study established a novel framework integrating data-driven pattern recognition of DBPs pollution with cellular biomechanical response evaluation. By analyzing extensive monitoring data from 12 water treatment plants, we identified four distinct DBPs pollution patterns with characteristic compositional profiles and seasonal variations. Most significantly, Pattern 4 (Emerging DBPs enriched) and Pattern 3 (Brominated DBPs enriched) induced the most pronounced biomechanical alterations across all tested cell types, with effects detectable at concentrations substantially lower than those required for conventional cytotoxicity. The multi-parametric biomechanical analysis revealed that these DBPs patterns caused significant cytoskeletal reorganization, increased cellular stiffness, reduced deformability, and impaired migration capacity, with kidney epithelial cells (HK-2) showing the highest sensitivity. These findings suggest that cellular biomechanical parameters could serve as sensitive early indicators of DBPs-induced effects, potentially addressing a critical gap in current risk assessment approaches.

The observed pattern-specific relationships between DBPs composition and biomechanical responses provide important insights for drinking water safety management. The strong effects of emerging unregulated DBPs at environmentally relevant concentrations emphasize the need for expanded monitoring beyond regulated compounds. Meanwhile, the identified pollution patterns offer a foundation for developing targeted treatment strategies and predictive models for DBPs formation control. Future research should focus on validating these biomechanical effects in more complex tissue models and epidemiological studies, establishing mechanistic links between cellular alterations and adverse health outcomes, and developing integrated risk assessment frameworks incorporating both chemical and biomechanical indicators. This interdisciplinary approach opens new avenues for understanding and mitigating the health risks associated with complex DBPs mixtures in drinking water, ultimately contributing to more effective water safety management strategies.

Author contributions: Conceptualization, RZ and YZ; methodology, RZ; software, RZ and YZ; validation, RZ and YZ; formal analysis, RZ and YZ; investigation, RZ and YZ; resources, JL; data curation, RZ and YZ; writing—original draft preparation, RZ; writing — review and editing, RZ, YZ and JL; visualization, RZ and TZ; supervision, JL; project administration, JL; funding acquisition, JL. All authors have read and agreed to the published version of the manuscript.

Ethical approval: Not applicable.

Informed consent statement: Not applicable.

Conflict of interest: The authors declare no conflict of interest.

References

1. Li XF, Mitch WA. Drinking Water Disinfection Byproducts (DBPs) and Human Health Effects: Multidisciplinary Challenges and Opportunities. Environmental Science & Technology. 2018; 52(4): 1681-1689. doi: 10.1021/acs.est.7b05440
2. Kalita I, Kamilaris A, Havinga P, et al. Assessing the Health Impact of Disinfection Byproducts in Drinking Water. ACS ES&T Water. 2024; 4(4): 1564-1578. doi: 10.1021/acsestwater.3c00664
3. Stalter D, O'Malley E, von Gunten U, et al. Mixture effects of drinking water disinfection by-products: implications for risk assessment. Environmental Science: Water Research & Technology. 2020; 6(9): 2341-2351. doi: 10.1039/c9ew00988d
4. Chen Y, Liang Q, Liang W, et al. Identification of Toxicity Forcing Agents from Individual Aliphatic and Aromatic Disinfection Byproducts Formed in Drinking Water: Implications and Limitations. Environmental Science & Technology. 2023; 57(3): 1366-1377. doi: 10.1021/acs.est.2c07629
5. Qiu T, Shi W, Chen J, et al. Haloketones: A class of unregulated priority DBPs with high contribution to drinking water cytotoxicity. Water Research. 2024; 259: 121866. doi: 10.1016/j.watres.2024.121866
6. Wei X, Yang M, Zhu Q, et al. Comparative Quantitative Toxicology and QSAR Modeling of the Haloacetonitriles: Forcing Agents of Water Disinfection Byproduct Toxicity. Environmental Science & Technology. 2020; 54(14): 8909-8918. doi: 10.1021/acs.est.0c02035
7. Zhang L, Qin J, Zhang Z, et al. Concentrations and potential health risks of methyl tertiary-butyl ether (MTBE) in air and drinking water from Nanning, South China. Science of The Total Environment. 2016; 541: 1348-1354. doi: 10.1016/j.scitotenv.2015.10.038
8. Wang W, Qian Y, Boyd JM, et al. Halobenzoquinones in Swimming Pool Waters and Their Formation from Personal Care Products. Environmental Science & Technology. 2013; 47(7): 3275-3282. doi: 10.1021/es304938x
9. Chen Z, Yang L, Li Z, et al. Application of biomarkers in the study of the health effects of disinfection by-products. Current Opinion in Environmental Science & Health. 2019; 7: 108-116. doi: 10.1016/j.coesh.2019.01.002
10. Yang L, Chen X, She Q, et al. Regulation, formation, exposure, and treatment of disinfection by-products (DBPs) in swimming pool waters: A critical review. Environment International. 2018; 121: 1039-1057. doi: 10.1016/j.envint.2018.10.024
11. Darling EM, Di Carlo D. High-Throughput Assessment of Cellular Mechanical Properties. Annual Review of Biomedical Engineering. 2015; 17(1): 35-62. doi: 10.1146/annurev-bioeng-071114-040545
12. Guo Q, Park S, Ma H. Microfluidic micropipette aspiration for measuring the deformability of single cells. Lab on a Chip. 2012; 12(15): 2687. doi: 10.1039/c2lc40205j
13. Mukherjee R, Saha M, Routray A, et al. Nanoscale Surface Characterization of Human Erythrocytes by Atomic Force Microscopy: A Critical Review. IEEE Transactions on NanoBioscience. 2015; 14(6): 625-633. doi: 10.1109/tnb.2015.2424674
14. Alcaraz J, Otero J, Jorba I, et al. Bidirectional mechanobiology between cells and their local extracellular matrix probed by atomic force microscopy. Seminars in Cell & Developmental Biology. 2018; 73: 71-81. doi: 10.1016/j.semcdb.2017.07.020
15. Tang G, Galluzzi M, Zhang B, et al. Biomechanical Heterogeneity of Living Cells: Comparison between Atomic Force Microscopy and Finite Element Simulation. Langmuir. 2018; 35(23): 7578-7587. doi: 10.1021/acs.langmuir.8b02211
16. Liu T, Zhang M, Wen D, et al. Temporal and spatial variations of disinfection by-products in South Taihu's drinking water,

Zhejiang Province, China. Journal of Water and Health. 2023; 21(10): 1503-1517. doi: 10.2166/wh.2023.149

17. Yu Y, Hossain MdM, Sikder R, et al. Exploring the potential of machine learning to understand the occurrence and health risks of haloacetic acids in a drinking water distribution system. Science of The Total Environment. 2024; 951: 175573. doi: 10.1016/j.scitotenv.2024.175573
18. Cortés-Eslava J, Gómez-Arroyo S, Risueño MC, et al. The effects of organophosphorus insecticides and heavy metals on DNA damage and programmed cell death in two plant models. Environmental Pollution. 2018; 240: 77-86. doi: 10.1016/j.envpol.2018.04.119
19. Mandal A, Giri S, Giri A. Assessment of toxicity, genotoxicity and oxidative stress in Fejervarya limnocharis exposed to tributyltin. Environmental Science and Pollution Research. 2024; 31(10): 14938-14948. doi: 10.1007/s11356-024-32220-5
20. Khani L, Martin L, Pułaski Ł. Cellular and physiological mechanisms of halogenated and organophosphorus flame retardant toxicity. Science of The Total Environment. 2023; 897: 165272. doi: 10.1016/j.scitotenv.2023.165272
21. Wang J, Liu T, Liu L, et al. Immune dysfunction induced by 2,6-dichloro-1,4-benzoquinone, an emerging water disinfection byproduct, due to the defects of host-microbiome interactions. Chemosphere. 2022; 294: 133777. doi: 10.1016/j.chemosphere.2022.133777